IIAT Instituto Internacional de Análise Térmica

Available online at www.bjta.com.br
Braz. J. Therm. Anal. Vol. 2 No. 1 (2013) 23 - 30

Brazilian Journal of Thermal Analysis BJTA

Synthesis, Characterization and Thermal Behavior of Solid-State Compounds of Light Trivalent Lanthanide Malonates

J. R. Locatelli[1]; F. J. Caires[2]; E. Y. Ionashiro[3]; C. T. Carvalho[4*]

[1]*Academia da Força Aérea (AFA) - Pirassununga-SP, Brazil.*
[2]*Instituto de Química, Universidade Estadual Paulista, 14801-970 -Araraquara-SP, Brazil.*
[3]*Universidade Federal de Goiás, 74001-970 - Goiânia-GO, Brazil.*
[4]*Universidade Federal da Grande Dourados, 79.804-970 - Dourados-MS, Brazil.*

Received 07/05/2013; accepted 11/12/2013
Available online 18/12/2013

Abstract

In this study, compounds of hydrated lanthanide malonates were synthesized by precipitation of sodium malonates ion. Quantitative studies of the compounds obtained in the solid state, as well as the thermal behavior of these compounds were performed by thermal analysis (TG-DTA and DSC). Additional complementary studies were also performed using X-ray diffraction by the powder method (XRD), Evolved Gas Analysis (EGA) and complexometric titration with EDTA. Thus, the compounds synthesized in this work, ranging from lanthanum to gadolinium, were studied mainly in relation to their thermal properties, enabling to establish the stoichiometry, the decomposition steps and identify by EGA the main volatile products released during the decomposition. The qualitative study by XRD and FT-IR showed that the compounds were obtained in the crystalline state and metal-ligand coordination occurs by bidentate bonding and /or bridge, respectively. The interest in these compounds is due to the several applications of malonate ion, such as industrial and biological, not to mention that the coordination of the lanthanide ions to the malonate ligand can provide them new properties which could be studied and explored forward.

Keywords: rare earths; malonates; TG-DTA; FT-IR

1. Introduction

Malonate compounds have been extensively studied in the solid state, especially with transition metals. Studies have mainly aimed at the synthesis, characterization of the crystalline structure, type of coordination, thermal decomposition, magnetic and spectroscopic properties [1-3]. As the malonate is a short chain dicarboxylic binder, it can coordinate to the metal chelate forming a six-membered ring, or act as a monodentate or bidentate ligand. Therefore, this kind of binder is often used to ensure a good prediction of the crystal structure and versatility of the structure when coordinated to the metal [4]. However, lanthanide malonates are poorly studied in relation to the applications mentioned for transition metals, since lanthanide compounds have mainly been studied because of their spectroscopic and magnetic properties. These properties have enabled the use of this material in different areas of commercial interest, once they can be intensified depending on the organic ligand coordinated to the lanthanide ion [5-13].

In this paper, the compounds of the light trivalent lanthanide malonates (La - Gd) were investigated following the previous work of the heavy trivalent lanthanides (Tb - Lu) [14]. The characterization of the synthesized compounds was performed using thermoanalytical techniques, infrared spectroscopy and complementary techniques. This study reports on the thermal stability of anhydrous and hydrated compounds, thermal decomposition and formation of intermediate compounds in air atmosphere, as well as the spectroscopic study of anti-symmetric and symmetric stretching modes of the carboxylate groups [15].

2. Experimental

General information and instrumental measurements

The sodium malonate monohydrated, $Na_2CH_2C_2O_4.H_2O$ with 99.6 % purity was obtained from Sigma, and aqueous solution of 0.1 mol L^{-1} was prepared, by direct weighing of the salt.

In the solid state compounds hydration water, ligand and metal ion contents were determined from TG curves. The metal ions were also determined by complexometric tritrations with standard EDTA solution using xylenol orange as indicator [16, 17], after igniting the compounds to respective oxides and dissolving them in hydrochloric acid solution. Carbon and hydrogen contents were determined by microanalytical procedures, with an EA 1110 CHNS-O Elemental Analyser from CE Instruments.

X-ray powder patterns were obtained using a Siemens D-5000 X-ray diffractometer, employing CuKα radiation (λ = 1.541Å) and a setting of 40 kV and 20 mA.

The attenuate total reflectance infrared spectra for sodium malonate, as well as for its metal-ion compounds were run on a Nicolet iS10 FT-IR spectrophotometer, using an ATR accessory with Ge window.

Simultaneous TG-DTA and DSC curves were obtained with two thermal analysis system, model SDT 2960 and DSC Q10, both from TA Instruments. The purge gas

*** Corresponding author:** Tel.: +55 67-3411-3894
E-mail address: claudiocarvalho@ufgd.edu.br (C. T. Carvalho)

doi: s/n

was an air with a flow rate of 100 mL min^{-1} for TG-DTA and 50 mL min^{-1} for DSC experiments. A heating rate of 20 K min^{-1} was adopted, with sample masses about 5.0 mg for TG-DTA and 2.0 mg for DSC runs. Alumina and aluminium crucibles, the latter with perforated cover, were used for TG-DTA and DSC, respectively.

The measurements of the gaseous products were carried out using a Thermogravimetric Analyzer Mettler TG-DSC coupled to a FT-IR spectrophotometer Nicolet with gas cell and DTGS KBr detector. The furnace and the heated gas cell (523 K) were coupled through a heated (T = 473 K) 120 cm stainless steel line transfer with diameter 2 mm both purged with dry air (50 mL min^{-1}). The FT-IR spectra were recorded with 16 scans per spectrum at a resolution of 4 cm^{-1}.

Compound preparations

Lanthanide(III) chlorides were prepared from the corresponding metal oxides, except for cerium, by treatment with concentrated hydrochloric acid. The resulting solutions were evaporated to near dryness; the residues were again dissolved in distilled water, transferred to a volumetric flask and diluted in order to obtain ca. 0.1 mol L^{-1} solutions, whose pH were adjusted to 5.0 by adding diluted sodium hydroxide solution. Cerium(III) was used as its nitrate and ca. 0.1 mol L^{-1} aqueous solution of this ion was prepared by direct weighing of the salt.

The solid-state compounds were prepared by adding slowly, with continuous stirring, the aqueous solutions of the ligand ($Na_2CH_2C_2O_4$) to the respective metal chloride or nitrate solution until total precipitation of the metal ions. The precipitates were washed with distilled water until elimination of chloride or nitrate ions, filtered through and dried on Whatman no. 42 filter paper and kept in desiccator over anhydrous calcium chloride.

3. Results and Discussions

Stoichiometry

The analytical and thermoanalytical (TG) results of the synthesized compounds are shown in Table 1. These results permitted to establish the stoichiometry of these compounds, which is in agreement with the general formula: $Ln_2(CH_2C_2O_4)_3{\cdot}nH_2O$, where Ln = La to Gd, except Pm, $(CH_2C_2O_4)_3$ is malonate, and n = 4.5 (La, Ce), 6 (Pr, Nd, Sm, Eu), 7 (Gd).

X - Ray Powder

The X - ray powder patterns Fig. 1 show that all the compounds have a crystalline structure and Nd, Sm and Eu compounds with evidence for formation of an isomorphous series. The X-ray powder patterns also show that the final residues of these compounds are: La_2O_3, CeO_2, Pr_6O_{11}, Nd_2O_3, Sm_2O_3, Eu_2O_3 and Gd_2O_3, respectively.

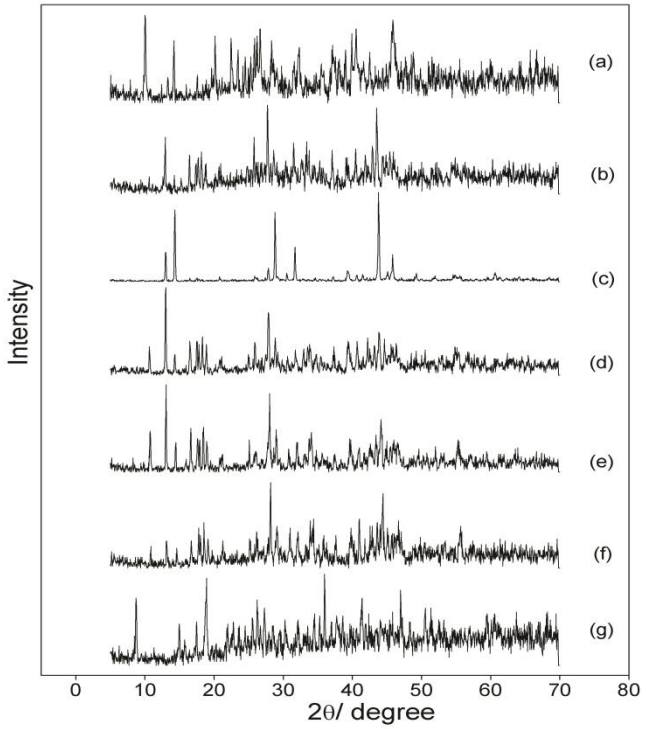

Figure 1. X-ray powder diffraction patterns of the compounds: (a) $La_2(L)_3{\cdot}4.5H_2O$, (b) $Ce_2(L)_3{\cdot}4.5H_2O$, (c) $Pr_2(L)_3{\cdot}6H_2O$, (d) $Nd_2(L)_3{\cdot}6H_2O$, (e) $Sm_2(L)_3{\cdot}6H_2O$, (f) $Eu_2(L)_3{\cdot}6H_2O$ and (g) $Gd_2(L)_3{\cdot}7H_2O$. (L= malonate).

FT-IR

The attenuate total reflectance spectroscopic data on malonate and its compounds with the metal ions considered in this work are shown in Table 2. The investigation was focused mainly within 1700-1400 cm^{-1} range because this region is potentially most informative in attempting to assign coordination site.

In $Na_2CH_2C_2O_4$, strong band at 1582 cm^{-1} and a medium intensity band located at 1352 cm^{-1} are attributed to the anti-symmetrical and symmetrical frequencies of the carboxylate groups, respectively. The band assigned to the anti-symmetrical stretching carboxylate frequencies are shifted to lower values relative to the corresponding frequencies in $CH_2C_2O_4$ itself (sodium salt) and $\Delta\nu$(OCO) significantly less than ionic value. This behavior indicates that the coordination carried out through the carboxylate group [18] and the infrared spectra data suggests that the bonding of the carboxylate group to the metal is chelating bidentate and/or bridging in these compounds [19]. The appearance of two ν_{sym} (OCO) bands in the spectrum of lanthanum and gadolinium compounds is probably due to different types of interaction between the carboxylate groups of malonate and these metal ions. All the conclusions are supported (in the case of the La, Pr, Nd, Sm, Eu and Gd compounds) by the results of the crystal structure determination [20 - 25].

Table 1. Analytical, thermoanalytical (TG) and elemental analysis data of the compounds $Ln_2(L)_3 \cdot nH_2O$.

Compounds	Ln^*(%)			L^{**} (lost)/ (%)		H_2O/ (%)		C%		H%		Final Residue
	Calcd.	TG	EDTA	Calcd.	TG	Calcd.	TG	Calcd.	E.A.	Calcd.	E.A.	
$La_2(L)_3 \cdot 4.5H_2O$	41.77	42.11	42.29	38.82	38.03	12.19	12.40	16.25	16.59	2.28	2.33	La_2O_3
$Ce_2(L)_3 \cdot 4.5H_2O$	41.98	42.07	41.39	36.29	36.38	12.14	12.24	16.19	16.14	2.27	2.40	CeO_2
$Pr_2(L)_3 \cdot 6H_2O$	40.49	39.71	39.66	35.56	35.97	15.53	15.75	15.52	15.34	2.61	2.30	Pr_6O_{11}
$Nd_2(L)_3 \cdot 6H_2O$	41.05	40.90	40.60	36.73	36.91	15.39	15.38	15.38	15.46	2.59	2.30	Nd_2O_3
$Sm_2(L)_3 \cdot 6H_2O$	42.06	42.10	42.12	36.11	36.01	15.12	15.17	15.12	15.20	2.54	2.40	Sm_2O_3
$Eu_2(L)_3 \cdot 6H_2O$	42.32	42.33	42.55	35.94	35.64	15.05	15.29	15.05	15.18	2.53	2.46	Eu_2O_3
$Gd_2(L)_3 \cdot 7H_2O$	42.11	42.07	42.22	34.57	35.04	16.89	16.81	14.47	14.67	2.70	2.51	Gd_2O_3

* trivalent lanthanides; ** malonate

Table 2. Spectroscopic data for sodium malonates ($Na_2CH_2C_2O_4$) and compounds with lighter trivalent lanthanides.

Compound	ν_{as} (COO^-) /cm^{-1}	ν_{sym} (COO^-) /cm^{-1}	$\Delta\nu$ (ν_{as} - ν_{sym}) /cm^{-1}
$Na_2L{\cdot}H_2O$	1582_{vs}	1354_{m}	228
$La_2L_3{\cdot}4.5H_2O$	1537_{vs}	1370 1348_{s}	167 189
$Ce_2L_3{\cdot}4.5H_2O$	1556_{vs}	1376_{s}	180
$Pr_2L_3{\cdot}6H_2O$	1551_{vs}	1377_{s}	174
$Nd_2L_3{\cdot}6H_2O$	1557_{vs}	1379_{s}	178
$Sm_2L_3{\cdot}6H_2O$	1558_{vs}	1381_{s}	177
$Eu_2L_3{\cdot}6H_2O$	1559_{vs}	1382_{s}	177
$Gd_2L_3{\cdot}7H_2O$	1563_{vs}	1373 1350_{m}	190 213

Thermal Analysis

The simultaneous TG-DTA curves of the compounds are shown in Fig. 2. These curves show mass losses in three, four or five consecutive and/or overlapping steps and thermal events corresponding to these losses.

The thermal behavior of the compounds is heavily dependent on the nature of the lanthanide ion and so the features of each of these compounds are discussed individually.

Lanthanum compound

The simultaneous TG-DTA curves are shown in Fig. 2a. These curves show mass losses in five steps and endothermic or exothermic peaks corresponding to these losses. The first two mass losses between 303-377 K and 377-493 K, corresponding to the endothermic peaks at 375 K and 420 K are due to dehydration with losses of 1.5 and 3 H_2O, respectively (Calc. = 4.06 and 8.13 %, TG = 4.33 and 8.07 %).

The thermal decomposition of the anhydrous compound occurs in three steps between 573-683 K, 683-846 K and 846-1023 K, with losses of 21.56 %, 8.23 % and 8.24 %, respectively, corresponding to exothermic peaks at 676 K and 943 K attributed to oxidation of the organic matter and the endothermic peak at 990 K ascribed to the thermal decomposition of a derivative of carbonate formed as intermediate. The formation of this intermediate was confirmed by test with hydrochloric acid solution on sample heated up to the temperature, as indicated by the TG-DTA curves. The total mass loss up to 1023 K is in agreement with the formation of La_2O_3, as final residue (Calc.=51.01%, TG = 50.43 %)

Cerium compound

The simultaneous TG-DTA curves are shown in Fig. 2b. These curves show mass losses in three steps and thermal events corresponding to these losses. The first two mass losses between 303-378 K and 378-473 K, corresponding to the endothermic peaks at 385 and 421 K are due to dehydration with losses of 2 and 2.5 H_2O, respectively (Calc. = 5.40 %, 6.71 %; TG = 5.29 %, 6.95 %).

The thermal decomposition of the anhydrous compound occurs in a single step between 473-603 K with loss of 36.38%, corresponding to an exothermic peak at 596 K attributed to oxidation reaction of Ce(III) to Ce(IV) together with the oxidation of the organic matter. The total mass loss up to 603 K is in agreement with the formation of CeO_2, as final residue (Calc. = 48.43 %, TG = 48.62 %). The less thermal stability of the cerium compound is ascribed to the oxidation reaction of Ce(III) to Ce(IV), and this behavior have already been observed for other cerium compound [26].

Praseodymium compound

The simultaneous TG-DTA curves are shown in Fig. 2c. These curves show mass losses in five steps and thermal events corresponding to these losses. The first two overlapping mass losses between 273 and 493 K, corresponding to the endothermic peak at 423 K with shoulder at 483 K are due to dehydration with losses 6 H_2O (Calc. = 15.53 %, TG = 15.75 %). The anhydrous compound is stable up to 573 K and above this temperature the thermal decomposition occurs in three steps between 573-643 K, 643-663 K and 743-1053 K, with losses of 7.04 %, 19.81 % and 9.12 %, respectively, corresponding to an exothermic peak at 655 K attributed to the oxidation of organic matter. No thermal event corresponding to the first and third mass losses of the anhydrous compound is observed in DTA curve and this is probably due to the balance between an endothermic process (decomposition) and exothermic one (oxidation of the gaseous products evolved); the resulting net heats is not sufficient to produce a thermal event. The total mass loss up to 1053 K is in agreement with the formation of Pr_6O_{11}, as final residue (Calc. = 51.09 %, TG = 51.72 %).

Neodymium compound

The simultaneous TG-DTA curves are shown in Fig. 2d. These curves show mass losses in four steps and endothermic or exothermic peaks corresponding to these losses. The first mass loss between 373-473 K corresponding to an endothermic peak at 427 K is due to dehydration with loss of 6 H_2O (Calc. = 15.39 %; TG = 15,38 %).

The anhydrous compound is stable up to 553 K and above this temperature the thermal decomposition occurs in three steps between 553-728 K, 728-853 K and 853-943 K, with losses of 25.68 %, 6.42 % and 4.81 %, respectively, corresponding to the exothermic peaks at 625 K and 821 K attributed to the oxidation of the organic matter with formation of an intermediate derivative of carbonate, as already observed for lanthanum compound. The endothermic peak at 903 K is attributed to the thermal

decomposition of this intermediate. The total mass loss up to 943 K is in agreement with the formation of Nd_2O_3 as final residue (Calc. = 52.12 %, TG = 52.29 %).

Samarium compound

The simultaneous TG-DTA curves are shown in Fig. 2e. These curves show mass losses in five steps and thermal events corresponding to these losses. The first mass loss between 373-503 K, corresponding to a broad and large endothermic peak at 428 K is due to dehydration with loss of 6 H_2O (Calc. = 15.12 %, TG = 15.17 %). The anhydrous compound is stable up to 578 K and above this temperature the thermal decomposition occurs in four consecutive and/or overlapping steps. The first three mass losses between 578-643 K, 643-703 K and 703-1023 K, with losses of 8.61 %, 13.05 % and 12.00 %, respectively, corresponding to the exothermic peaks at 655 K and 923 K are attributed to the oxidation of the organic matter, with formation of a derivative of carbonate, too. The last mass loss between 1023-1173 K corresponding to an endothermic peak at 1071 K, with loss of 2.35 % is attributed to the thermal decomposition of this intermediate. The total mass loss up to 1173 K is in agreement with the formation of Sm_2O_3, as final residue (Calc. = 51.23 %, TG = 51.18 %).

Europium compound

The simultaneous TG-DTA curves are shown in Fig. 2f. These curves show mass losses in five steps and thermal events corresponding to these losses. The first two steps between 363-443 K and 443-503 K, corresponding to the overlapping endothermic peaks at 423 K and 476 K, are attributed to the dehydration with losses of 3 H_2O in each step (Calc. = 7.53 %, TG = 7.33 % and 7.86 %).

The anhydrous compound is stable up to 573 K and above this temperature the thermal decomposition occurs in three steps between 573-663 K, 663-848 K and 848-1003 K, with losses of 15.96 %, 15.96 % and 3.72 %, respectively, corresponding to the exothermic peaks at 648 K, 656 K and 741 K attributed to the oxidation of the organic matter. No thermal event corresponding to the last mass loss is observed in the DTA curve, as already observed for the praseodymium compound. The total mass loss up to 1003 K is in agreement with the formation of Eu_2O_3, as final residue (Calc. = 50.99 %, TG = 50.83 %).

Gadolinium compound

The simultaneous TG-DTA curves are shown in Fig. 2g. These curves show mass losses in three steps and thermal events corresponding to these losses. The first mass loss between 343-383 K, corresponding to a large endothermic peak at 409 K is due to dehydration with loss of 7 H_2O (Calc. = 16.89 %, TG = 16.81 %).

The anhydrous compound is stable up to 553 K and above this temperature the thermal decomposition occurs in two steps between 553-703 K and 703-1053 K, with losses of 20.17 % and 14.87 %, respectively, corresponding to the exothermic peaks at 652 and 961 K attributed to the oxidation of the organic matter. The total mass loss up to 1053 K is in agreement with the formation of Gd_2O_3, as final residue (Calc. = 51.46 %, TG = 51.85 %).

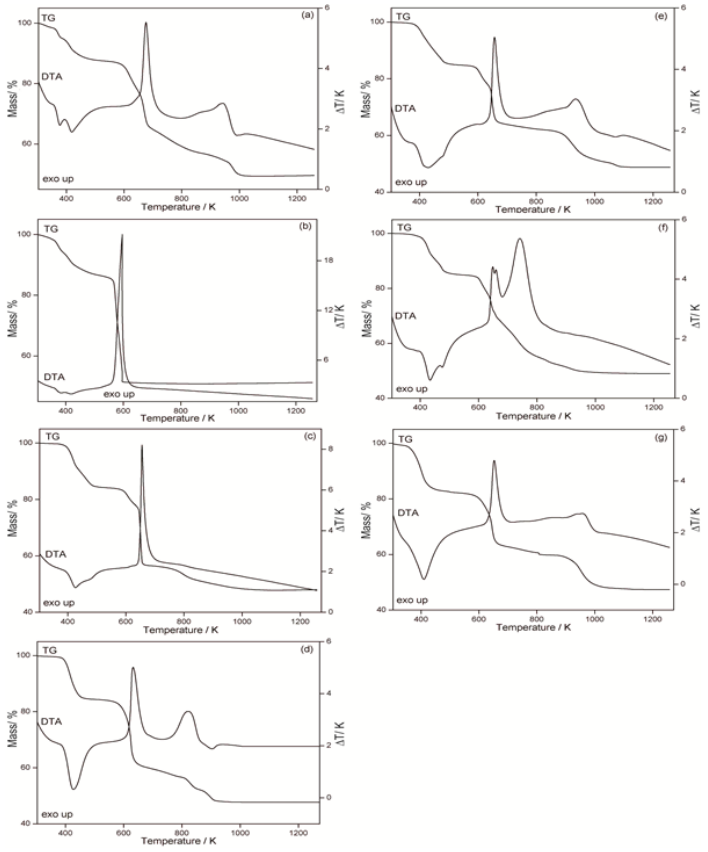

Figure 2. Simultaneous TG-DTA curves of the compounds: (a) $La_2(L)_3{\cdot}4.5H_2O$ (m = 5.13 mg), (b) $Ce_2(L)_3{\cdot}4.5H_2O$ (m = 5.10 mg), (c) $Pr_2(L)_3{\cdot}6H_2O$ (m = 3.52 mg), (d) $Nd_2(L)_3{\cdot}6H_2O$ (m = 5.22 mg), (e) $Sm_2(L)_3{\cdot}6H_2O$ (m = 5.27 mg), (f) $Eu_2(L)_3{\cdot}6H_2O$ (m = 5.21 mg) and (g) $Gd_2(L)_3{\cdot}7H_2O$ (m = 5.06 mg). (L = malonate)

Considerations Thermal Decomposition of Compounds (TG-DTA)

The formation of a derivative of carbonate, as observed in the thermal decomposition of lanthanum, neodymium and samarium compounds, was not observed during the thermal decomposition of cerium, praseodymium, europium and gadolinium ones. For the cerium and praseodymium compounds this is undoubtedly related to the oxidation reaction of Ce(III) to Ce(IV) and Pr(III) to Pr_6O_{11} together with the oxidation of the organic matter, both exothermic processes and for europium and gadolinium compounds due to the oxidation of the organic matter and a decreasing stability of this intermediate with increasing atomic number of the lanthanide ions [26].

The TG-DTA profiles, as well as the temperature range and the mass losses observed in each step of the TG curve are in disagreement with the results reported by Muraishi and co-workers [27]. These disagreements undoubtedly are due to the different experimental conditions, principally the static air atmosphere used to obtain the TG and DTA curves. For the dynamic atmosphere the evolved products of the thermal decompositions are

continuously changed while in the static atmosphere the same is not observed. On that account the disagreements are observed.

Differential Scanning Calorimetry (DSC)

The DSC curves of the compounds are shown in Fig. 3. These curves show endothermic and exothermic peaks that all are in agreement with the mass losses observed in the TG curves. Small differences observed concerning the peak temperatures obtained by TG-DTA and DSC are undoubtedly due to the perforated cover used to obtain the DSC curves, while TG-DTA ones are obtained without cover, beyond the experimental conditions that were not the same.

The endothermic peaks up to 498 K are due to dehydration, which occurs in a single (Ce, Nd, Gd), two (La) or two overlapping steps (Pr, Sm, Eu). The dehydration enthalpies found for these compounds were: 47.2 and 87.1 (La), 231.1 (Ce), 268.1 (Pr), 303.0 (Nd), 303.3 (Sm), 235.9 (Eu) and 244.6 (Gd) kJ mol^{-1}.

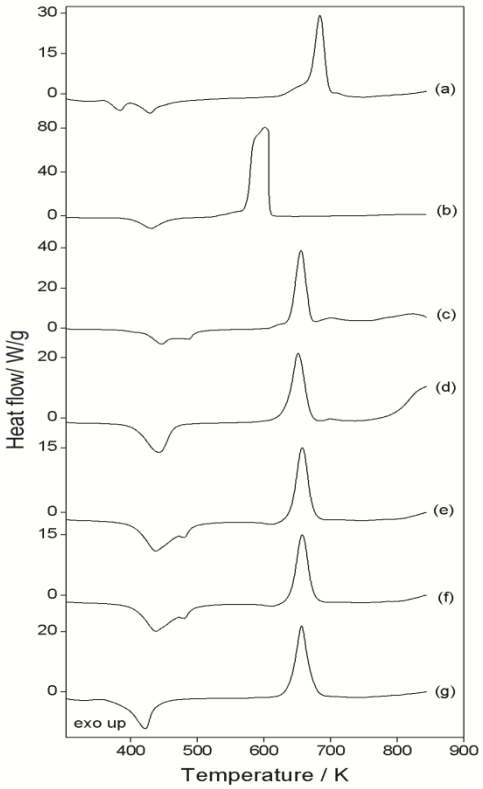

Figure 3. DSC curves of the compounds: (a) $La_2(L)_3{\cdot}4.5H_2O$ (m = 2.22 mg), (b) $Ce_2(L)_3{\cdot}4.5H_2O$ (m = 2.03 mg), (c) $Pr_2(L)_3{\cdot}6H_2O$ (m = 2.28 mg), (d) $Nd_2(L)_3{\cdot}6H_2O$ (m = 2.05 mg), (e) $Sm_2(L)_3{\cdot}6H_2O$ (m = 2.17 mg), (f) $Eu_2(L)_3{\cdot}6H_2O$ (m = 2.26 mg) and (g) $Gd_2(L)_3{\cdot}7H_2O$ (m = 2.01 mg). (L= malonate).

Gas Analysis (FT-IR)

The gaseous products evolved during the thermal decomposition in an air atmosphere of the compounds studied in this work were monitored by FT-IR, and they have acetone and carbon dioxide as main products undoubtedly due to decarboxylation and oxidation of the organic matter. The IR spectra of the gaseous products evolved during the thermal decomposition of lanthanum malonate, as representative of all the compounds, are shown in Fig. 4(a) and (b). The Fig 4(a) shows the IR spectrum of the gaseous products evolved between 573-673 K, the bands with peaks at 2360 cm^{-1} and 666 cm^{-1} are assigned to asymmetric stretch and scissoring (degenerated) vibrations, respectively that are attributed to carbon dioxide. The bands with peaks at 1737 cm^{-1} , 1366 cm^{-1} and 1215 cm^{-1} are assigned to the stretching vibration of C=O, angular symmetric deformation vibration of CH_3 group and stretching and angular deformation vibration of C–CO–C group, respectively that are attributed to acetone. The Figure 4b shows the FTIR spectrum of decomposition products (TG) between 673-1000 K and it has only CO_2.

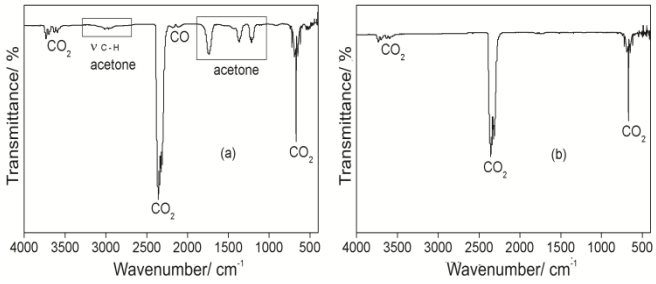

Figure 4. FT-IR spectra of gaseous products evolved during the thermal decomposition of lanthanum malonate, as representative of the all compounds, between (a) 573 – 673 K and (b) 673-1000.

Conclusions

From TG, complexometry and elemental analysis data, a general formula could be established for the synthesized compounds.

The TG-DTA and DSC curves provided previously unreported information about the thermal stability and thermal decomposition of these compounds in dynamic air atmosphere.

The X-ray powder patterns pointed out that the synthesized compounds have a crystalline structure and infrared spectroscopic data suggests that $CH_2C_2O_4$ acts as a chelating bidentate and/or briding bidentate ligand towards the metal ions considered in this work.

The study by gas analysis shows that the released gaseous products are similar at determinate temperature ranges. The peaks in the FTIR spectrum are due to water of hydration, carbon dioxide as main product, a small amount of carbon monoxide and acetone.

Acknowledgements

The authors thank, Ivo Giolito Thermal Analysis Laboratory (LATIG) and AFA, FAPESP, CNPq and CAPES Foundations for financial support.

References

[1] Delgado FS, Lahoz F, Lloret F, Julve M, Ruiz-Pérez C. Supramolecular Networks in Copper(II) Malonate Complexes. Cryst. Growt. & Des. 2008:8:3219-32. [Google Scholar] [CrossRef]

[2] Cui GH, Li JR, Hu TL, Bu XH. Synthesis, characterization and crystal structures of two discrete Cu(II) complexes with mixed-ligands: $[Cu(mal)(L)(H_2O)]\cdot H_2O$ and $[Cu(Phmal)(L)_2]$ (mal=malonate dianion, phmal=phenylmalonate dianion and L=5,5′-dimethyl-2,2′-bipyridine). J. Mol. Struc. 2005:738(1-3):183-7. [Google Scholar] [CrossRef]

[3] Caires FJ, Lima FS, Carvalho CT, Giagio RJ, Ionashiro M. Thermal behaviour of malonic acid, sodium malonate and its compounds with some bivalent transition metal ions. Thermochim. Acta 2010:497(1-2):35-40. [Google Scholar] [CrossRef]

[4] Déniz M, Hernández-Rodríguez I, Pasán J, Fabelo O, Cañadillas-Delgado L, Yuste C, Julve M, Lloret F, Ruiz-Pérez C. Pillaring Role of 4,4′-Azobis(pyridine) in Substituted Malonate- Containing Manganese(II). Complexes: Syntheses, Crystal Structures, and Magnetic Properties. Cryst. Growt. & Des. 2012:12(9):4505-18. [Google Scholar] [CrossRef]

[5] Kolechko DV, Kolokolov FA, Oflidi AI, Pikula AA, Panyushkin VT, Mikhailov IE, Dushenko GA. Novel luminescent lanthanides complexes with 1,10- phenanthroline-2,9-dicarboxylic acid. Dokl. Chem. 2011:441(2):374-8. [Google Scholar] [CrossRef]

[6] Leif R. C., Vallarino L. M., Bec M. C., Yang S. Increasing the luminescence of lanthanide complexes. Cytometry Part A 2006:69A(8):767-78. [Google Scholar] [Visualizar Item] [CrossRef]

[7] Martins TS, Isolani PC. Terras Raras: Aplicações Industriais e Biológicas. Quím. Nova. 2005:28(1):111-17. [Google Scholar] [Visualizar Item] [CrossRef]

[8] Li M, Ganea GM, Lu C, De Rooy SL, El-Zahab B, Fernand VE, Jin R, Aggarwal S, Warner IM. Lipophilic phosphonium–lanthanide compounds with magnetic, luminescent, and tumor targeting properties. J. Inorg. Biochem. 2012:107(1):40-46. [Google Scholar] [PubMed] [CrossRef]

[9] Langley SK, Chilton NF, Gass IA, Moubaraki B, Murray KS. Planar tetranuclear lanthanide clusters with the Dy4 analogue displaying slow magnetic relaxation. Dalton Trans. 2011:40(47):12656-59. [Google Scholar] [Visualizar Item] [PubMed] [CrossRef]

[10] Aime S, Bettinelli M, Ferrari M, Razzano E, Terreno E. NMR and luminescence studies on the formation of ternary adducts between HSA and Ln(III)–malonate complexes (Ln=Eu, Gd, Tb). Biochim. Biophy. Acta, Prot. Struct. Mol. Enzy. 1998:1385(1):7-16. [Google Scholar] [Visualizar Item] [PubMed] [CrossRef]

[11] Konstantina EC, Perlepes SP, Terzis A, Raptopoulou CP. Synthesis, crystal structures and spectroscopic studies of praseodymium(III) malonate complexes. Polyhedron 2010:29(16):3118-124. [Google Scholar] [CrossRef]

[12] Psuja P, Streket W. Influence of concentration and sintering temperature on luminescence properties of Eu^{3+}:SnO_2 nanocrystallites. J. Rare Earths. 2012:30(7):627-31. [Google Scholar] [Visualizar Item] [CrossRef]

[13] Tianliang Z, Zhen S, Liu B, Qingyong R, Quanlin L. Synthesis and luminescence properties of europium activated $Ca_3Al_2O_6$-$Sr_3Al_2O_6$ system. J. Rare Earths. 2012:30(7):632-36. [Google Scholar] [CrossRef]

[14] Locatelli JR, Carvalho CT, Caires FJ, Ionashiro M. Synthesis, characterization and thermal behavior of heavy trivalent lanthanide malonates. Eclet. Quím. 2010:35(4):93-100. [Google Scholar] [Visualizar Item] [CrossRef]

[15] Ribeiro KL, Trindade MAG, Carvalho AE, Arruda EJ, Carvalho CT. Synthesis, characterization and thermal behaviour of light trivalent lantahanide 3,4-(methylenedioxy)cinnamate. Braz. J. Therm. Anal. 2012:30-7. [Google Scholar]

[16] Flaschka HA. EDTA Titrations. Oxford: Pergamon Press; 1964. [Google Scholar]

[17] Ionashiro M, Graner CAF. Titulação Complexométrica de Lantanídeos e Ítrio. Eclet. Química. 1983:8:29-32. [Google Scholar]

[18] Nakamoto K. Infrared and Raman Spectra of Inorganic and Coordination Compounds, Part B. 5th. New York: Wiley; 1997. [Google Scholar]

[19] Deacon GB, Phillips RJ. Relationships between the carbon-oxygen stretching frequencies of carboxylate complexes and the type of carboxylate coordination. Coord. Chem. Rev. 1980:33(3):227-50. [Google Scholar] [CrossRef]

[20] Benmerad B, Guehria-Laïdoudi A, Bernardinelli G, Balegroune F. Polymeric tetraaquatris(malonato)dilanthanum(III) monohydrate. Acta Crystallogr., Sect. C: Struct. Chem. 2000:C56:321-23. [Google Scholar] [PubMed] [CrossRef]

[21] Hernández-Molina M, Lorenzo-Luis PA, López T, Ruiz-Pérez C, Lloret F, Julve M. Generation of lanthanide coordination polymers with dicarboxylate ligands: synthesis, structure, thermal decomposition and magnetic properties of the two-dimensional triaquatris(malonato)dipraseodymium(III) dihydrate {[$Pr_2(C_3H_2O_4)_3(H_2O)_3$]•$2H_2O$}. Cryst. Eng. Commum. 2000:2(31):169-73. [Google Scholar] [CrossRef]

[22] Doreswamy BH, Mahendra M, Sridhar MA, Shashidhara Prasad J, Varughese PA, George J., Varghese G. A novel three-dimensional polymeric structure of crystalline neodymium malonate hydrate. Mater. Lett. 2005:59(10):1206-213. [Google Scholar] [CrossRef]

[23] Wenmei X, Qiguang W, Lan Y, Rudong Y. Synthesis, characterization and crystal structure of tri-aquobimalonate malonate samarium(III) monohydrate. Polyhedron. 1992:11(16):2051-54. [Google Scholar] [CrossRef]

[24] Hansson E. Structural studies on the rare earth carboxylates. 17. Crystal and Molecular Structure of Hexa-Aquo Tris-malonato Di-neodymium(III) Dehydrate. Acta Chem. Scand. 1973:27:2441-54. [Google Scholar] [Visualizar Item] [CrossRef]

[25] Molina MH, Ruiz-Pérez C, López T, Lloret F, Julve M. Ferromagnetic Coupling in the Three-Dimensional Malonato-Bridged Gadolinium(III). Complex [$Gd_2(mal)_3(H_2O)_6$] (H_2mal = Malonic Acid). Inorg. Chem. 2003:42(18):5456-58. [Google Scholar] [Visualizar Item] [PubMed] [CrossRef]

[26] Locatelli JR, Rodrigues EC, Siqueira AB, Ionashiro EY. Characterization and Thermal Behaviour of Solid-State Compounds of Yttrium and Lanthanide Benzoates. J. Therm. Anal. Calorim. 2007:90(3):737-46. [Google Scholar] [Visualizar Item] [CrossRef]

[27] Muraishi K, Yokobayashi H, Nagase K. Systematics on the thermal reactions of lanthanide malonates $Ln_2(C_3H_2O_4)_3$•nH_2O in the solid state. Thermochim. Acta 1991:182(2):209-217. [Google Scholar] [Visualizar Item] [CrossRef]